The Journal of Neuroscience, November 1993, 13(11): 4609–4621

Stepwise Repolarization from Ca^{2+} Plateaus in Neocortical Pyramidal Cells: Evidence for Nonhomogeneous Distribution of HVA Ca^{2+} Channels in Dendrites

I. Reuveni, A. Friedman, Y. Amitai, and M. J. Gutnick

Department of Physiology, Corob Center for Medical Research, Faculty of Health Sciences, Ben Gurion University of the Negev, Beersheva 84105, Israel

Although cortical dendrites have classically been thought of as passive structures, recent evidence suggests that active conductances, including Ca^{2+} conductance, are also present in the dendritic membrane. To investigate this, we have recorded intracellularly in slices of rat neocortex bathed in 24 mM tetraethylammonium chloride and 1 μM TTX. Under these conditions, pyramidal neurons generated prolonged Ca^{2+} spikes. In computer simulations, the breakpoint voltage from which the plateau level began to repolarize was closely related to a specific region on the voltage/activation curve of the high-voltage-activated Ca^{2+} conductance underlying the spike. This modeling result was supported by the experimental observation that substituting Ba^{2+} for Ca^{2+} caused a hyperpolarizing shift in breakpoint voltage by 8–10 mV. Often there was stepwise repolarization from the Ca^{2+} spike to one or more additional plateau levels. In compartmental computer models, this could be simulated by two different mechanisms: (1) the presence of multiple, electrotonically separated sites of Ca^{2+} spike electrogenesis in the dendritic tree, and (2) the presence of Ca^{2+} channels with different voltage dependencies in the same compartment. In experiments, brief hyperpolarizing pulses could cut short the high-amplitude plateau without terminating the smaller "steps." This result could be simulated by both computer models. However, only the multicompartmental model could simulate effects of prolonged depolarizing and hyperpolarizing currents on the breakpoint. Thus, the more depolarized the breakpoint, and hence the closer the spike initiation zone to the recording site, the less it was affected by the injected current. In experiments, the ratio of the breakpoint voltages for the different plateau levels was equal to the ratio of the highest repolarization rates. These data indicate that the breakpoint voltage and the time course of repolarization were the same at all the sites of Ca^{2+} electrogenesis.

Our findings provide strong evidence that Ca^{2+} spike initiation occurs at electrotonically separated "hot spots" in the dendrites, and that voltage dependence of the Ca^{2+} channels that underlie the spikes is the same at all sites.

Received Oct. 7, 1992; revised Apr. 29, 1993; accepted May 6, 1993.

We thank Istvan Mody, John Huguenard, Idan Segev, and Ton Juta for helpful discussions and critical reading of the manuscript. This work was supported by a grant from the DFG (SFB 194).

Correspondence should be addressed to Michael J. Gutnick, D.V.M., Ph.D., Department of Physiology, Faculty of Health Sciences, Ben Gurion University of the Negev, Beersheva 84105, Israel.

[Key words: dendritic spikes, cortical pyramidal cells, calcium channels, calcium spikes, barium, hot spots, compartmental model]

The intrinsic integrative characteristics of a neuron are largely determined by the kinds of voltage-dependent ionic channels it possesses and by their spatial distribution in the somatic and dendritic membranes. Localization of channels relative to the electrotonic structure of the cell and to sites of its synaptic input is particularly significant in the case of Ca^{2+} conductance. Ca^{2+} current activation is not only a powerful electroresponsive mechanism; it is also an important means for regulating the intracellular concentration of Ca^{2+} ions, which themselves play a pivotal role in modulation of many critical cellular processes (Swanson, 1989). Since the diffusional mobility of Ca^{2+} ions in the cytoplasm is quite limited (Hodgkin and Keynes, 1957; McBurney and Neering, 1987; Connor et al., 1988; Sugimori and Llinas, 1990), while many Ca^{2+}-dependent processes are membrane bound (Imredy and Yue, 1992), knowing the site at which Ca^{2+} current is generated is essential to an understanding of its function in a particular neuron.

Of late, electrophysiological observations have provided strong evidence that in many central neurons, the dendritic arbor, the main synaptic surface of the cell, possesses voltage-dependent channels and is electrically excitable (Llinas and Nicholson, 1971; Wong et al., 1978; Llinas and Sugimori, 1980; Llinas and Yarom, 1981; Benardo et al., 1982; Jahnsen and Llinas, 1984; Masukawa and Prince, 1984; Stafstrom et al., 1985; Harris et al., 1989; Huguenard et al., 1989). In addition, imaging experiments with Ca^{2+}-sensing dyes (Ross and Werman, 1987; Connor et al., 1988; Tank et al., 1988; Jones et al., 1989; Ross et al., 1990; Sugimori and Llinas, 1990; Jaffe et al., 1992) and histochemical studies designed to stain specific membrane binding sites (Jones et al., 1989; Westenbroek et al., 1990; Hillman et al., 1991) have indicated the presence of dendritic Ca^{2+} channels. Most work in this field has concentrated on hippocampal pyramidal cells and cerebellar Purkinje cells, and less is known about Ca^{2+} conductance in the complex and elaborate dendritic trees of neocortical pyramidal cells. In dendritic intracellular recordings from neocortical cells, high-threshold, slow, TTX-resistant spikes are readily evoked by depolarizing current pulses (Amitai et al., 1993). However, in somatic recordings, although evidence of a transient, low-voltage-activated Ca^{2+} current is readily revealed (Friedman and Gutnick, 1987; Sutor and Zieglgansberger, 1987), evidence of high-voltage-activated (HVA)

current requires blockade of rectifying currents (Connors et al., 1982; Stafstrom et al., 1984).

Under conditions of K^+ current blockade with a high concentration of tetraethylammonium chloride (TEA), and Na^+ current blockade with TTX, brief somatic depolarizations evoke prolonged Ca^{2+} spikes in neocortical neurons, during which the membrane potential remains at a plateau level for seconds before rapid repolarization (Franz et al., 1986; Friedman and Gutnick, 1989; Friedman et al., 1992). Often, the repolarization phase is stepwise, and the membrane potential lingers at one or more intermediate plateau levels before returning to rest. This phenomenon has been seen in neurons from several other brain areas, and is generally taken to constitute evidence of electrotonic distant sites of Ca^{2+} spike electrogenesis with intervening patches of passive propagation (Llinas and Yarom, 1981; Leonard and Wickelgren, 1985). However, because there are many types of Ca^{2+} channels (Llinas et al., 1989; Tsien et al., 1991) and these may have different voltage dependencies, an alternative hypothesis is that the stepwise repolarization is caused by a mixture of channels of more than one type without spatial segregation.

In the present experiments, we have recorded in TTX and TEA and studied the stepwise repolarization phenomenon in detail, using computer simulation in parallel to design experiments and analyze our results. We were able to distinguish between the two hypotheses, and we conclude that the phenomenon indicates that in addition to a patch of Ca^{2+} electrogenesis at or near the soma, Ca^{2+} spikes are also generated at dendritic "hot spots" that are separated from the proximal patch of excitability and from each other by dendritic zones through which propagation is passive. Our findings indicate that although HVA channels are not evenly distributed in the soma–dendritic membrane of neocortical pyramidal cells, all have the same voltage dependence.

Portions of this research have appeared in abstract form (Reuveni et al., 1992).

Materials and Methods

Recording from neocortical slices in vitro. Techniques for preparing neocortical slices *in vitro* were as described elsewhere for this laboratory (Gutnick et al., 1985; Friedman and Gutnick, 1989; Friedman et al., 1992). Guinea pigs (250–400 gm) or rats (Sprague–Dawley, 100–200 gm) were anesthetized and decapitated. Their brains were quickly removed into cold (6°C) physiological solution. Blocks of parietal neocortex were dissected and glued to the cutting surface of a vibratome (Vibroslice), and coronal slices (nominally 400 μm thick) were cut from the area corresponding to the sensorimotor cortex. Slices were then placed in a recording chamber onto a lens paper–covered platform. Temperature was thermostatically held at 34–36°C, and humidified gas (95% O_2, 5% CO_2) flowed over the surface of the slices. Normal bathing solution contained (in mM) 124 NaCl, 5 KCl, 2 $CaCl_2$, 2 $MgSO_4$, 1.25 NaH_2PO_4, 26 $NaHCO_3$, and 10 dextrose, saturated with 95% O_2 and 5% CO_2. Na^+ currents were blocked with 1 μM tetrodotoxin (TTX), and K^+ currents with 24 mM tetraethylammonium chloride (TEA). Unless otherwise indicated, recording always commenced after at least 0.5 hr of incubation. During some experiments, $CaCl_2$ was replaced by an equimolar concentration of $BaCl_2$.

Glass microelectrodes were filled with 4 M potassium acetate and had impedances of about 60–80 MΩ. An Axoclamp-2A amplifier (Axon Instruments) was used in bridge mode. Data were stored on a PCM mode VCR recorder (Neurodata), digitized off line, and analyzed using pCLAMP (Axon Instruments).

Computer simulations. Computer simulations were based on the structure of a layer 5 neuron in the visual cortex of the rat. This cell had previously been intracellularly recorded, stained, reconstructed, and modeled by Stratford et al. (1989). Based on their measurements we represented the cell by a series of linked, isopotential segments (Segev et al., 1989) and simulated it with the program NEURON (Hines, 1989), implemented on a SUN SPARCstation IPC. For most runs, basilar dendrites and apical oblique dendrites were collapsed into simplified equivalent profiles (Stratford et al., 1989), such that the final model consisted of 100 segments. The electrical length of each segment was less than 0.1 space constant. The computational results presented here were obtained from simulations in which membrane parameters were assigned standard values of $C_m = 1\ \mu F/cm^2$, $R_m = 10{,}000\ \Omega \cdot cm^2$, and $R_i = 250\ \Omega \cdot cm$. In addition, a series of runs were also performed using higher dendritic R_m values and a considerable leak conductance at the soma, in line with recent modeling studies by Larkman et al. (1992). Parameter sets for these runs were

$$R_m = 15{,}020\ \Omega \cdot cm^2,\ R_i = 287\ \Omega \cdot cm,\ C_m = 1.1\ \mu F/cm^2;\ \text{somatic } g_{leak} = 4.7\ nS,$$

$$R_m = 21{,}000\ \Omega \cdot cm^2,\ R_i = 306\ \Omega \cdot cm,\ C_m = 1.0\ \mu F/cm^2;\ \text{somatic } g_{leak} = 7.9\ nS,$$

$$R_m = 32{,}870\ \Omega \cdot cm^2,\ R_i = 330\ \Omega \cdot cm,\ C_m = 0.9\ \mu F/cm^2;\ \text{somatic } g_{leak} = 10.9\ nS,$$

$$R_m = 65{,}900\ \Omega \cdot cm^2,\ R_i = 362\ \Omega \cdot cm,\ C_m = 0.8\ \mu F/cm^2;\ \text{somatic } g_{leak} = 13.7\ nS.$$

With standard parameters, membrane time constant $\tau_m = 10$ msec and input resistance was 70 MΩ (with the membrane entirely passive). These values were slightly different than the 16 ± 6 msec and 33 ± 13.6 MΩ (mean ± SD, $n = 32$) observed experimentally under these recording conditions. However, since these measurements reflected the characteristics of a heterogeneous population of neurons of different types and sizes, and since the simulation runs with the very different parameter sets specified above did not lead to different conclusions regarding the specific questions under study here, no great effort was made to mimic more precisely the experimentally determined neuronal properties. Some computations were made in an isopotential model that consisted of a single segment.

Spike electrogenesis was mediated by an HVA Ca^{2+} current with characteristics as described for neocortical neurons by Sayer et al. (1990). They reported that the current was maximal at voltages between −10 and −20 mV, where it reached a peak in 19 ± 7 msec. Based on their plot of the I/V characteristics of this Ca^{2+} conductance, Hodgkin and Huxley steady state activation variables and forward and backward rate constants (α and β, respectively) were derived. Rate functions (at 36°C) were

$$\alpha = \frac{0.055(-27 - V)}{e^{(-27-V)/3.8} - 1},$$

$$\beta = 0.94 \cdot e^{(-75-V)/17},$$

where V is membrane potential.

Voltage-dependent inactivation of the Ca^{2+} current was modeled after the data of Dichter and Zona (1989), who reported a very slow time constant of inactivation of around 500 msec. Inactivation rate functions were

$$\alpha = 0.000457 \cdot e^{(-13-V)/50},$$

$$\beta = \frac{0.0065}{e^{(-V-15)/28} + 1}.$$

Although there is good evidence for a prominent Ca^{2+}-dependent component to inactivation of this channel in cortical neurons (Friedman and Gutnick, 1989; Kay, 1991; Kohr and Mody, 1991), this was not included in the model since it would have complicated the simulations considerably while having no substantive effect on the conclusions.

Calcium current was modeled with m^2 activation kinetics (Kay and Wong, 1987), such that

$$I_{Ca} = \bar{g}_{Ca} \cdot m^2 \cdot h \cdot (V - E_{Ca}).$$

Wherever a Ca^{2+} conductance was inserted into the membrane, a K^+ conductance was also added. Of the afterhyperpolarization (AHP) currents that have been described for neocortical neurons, we chose to model the medium-duration afterhyperpolarization (mAHP) (Schwindt et al., 1988a). This current, which is very sensitive to apamine but only minimally affected by TEA, and is not voltage dependent, has a relatively short time course, which makes it most likely to have an effect on the duration of the Ca^{2+} spike. We used a model of the AHP current developed by Pennefather et al. (1990) based on data from frog sympathetic ganglion cells:

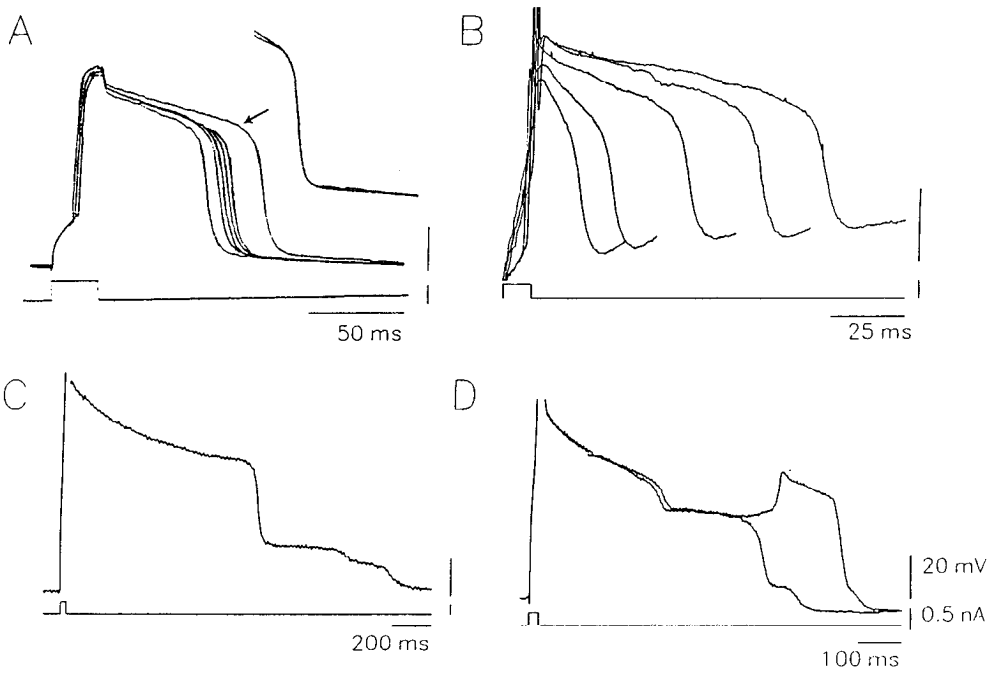

Figure 1. Ca^{2+} plateaus in slices bathed in TTX-TEA medium. *A*, Ca^{2+} spikes evoked by repetitive, brief, identical current pulses applied intracellularly at 0.1 Hz (six traces overlapped). Although the duration of the plateau varies from stimulus to stimulus, the breakpoint voltage (*arrow*) remains constant. *Inset*, The falling phases of these six traces were superimposed to show that the time course of repolarization is the same regardless of spike duration. *B*, The development of the Ca^{2+} spike as TTX-TEA medium washes into the chamber. The briefest trace was recorded 4 min after onset of wash-in, and the subsequent traces, recorded at 2 min intervals, became progressively prolonged. Note that breakpoint voltage is only minimally changed despite the large, progressive increase in relative Ca^{2+} conductance (as compared to conductances for Na^+ and K^+), which is indicated by increased peak amplitude of the plateau and reduction of the AHP. *C*, Stepwise repolarization of a Ca^{2+} spike, showing three distinct plateau voltages. *D*, Stepwise repolarization in a different neuron. Note that the voltage can flip from one plateau level to another.

$$\alpha = 200 - [Ca^{2+}]_i,$$
$$\beta = 0.0014,$$

where $[Ca^{2+}]_i$ is the millimolar concentration of Ca^{2+} in the outermost shell (see below). A very simplified model of radial diffusion, included in the NEURON program (Hines, 1989), was implemented as a mechanism to regulate $[Ca^{2+}]_i$. Three radial shells, of uniform thickness, were used; Ca buffer (8 mM) with an affinity of 10 μM was included in the shell nearest to the membrane. $[Ca^{2+}]_i$ was only modeled in active segments; lateral diffusion of calcium was not simulated. $[Ca^{2+}]_o$ was held at 2 mM and the initial value of $[Ca^{2+}]_i$ was 2.5 μM, yielding a reversal potential of 90 mV at 36°C.

Three different models are presented at various places in this article. Basic characteristics of Ca^{2+} spikes were explored in an isopotential model that consisted of a single compartment with the following conductance parameters: $g_{Ca,max}$ = 0.000535 S/cm²; $g_{K,max}$ = 0.0002 S/cm²; g_{leak} = 0.00035 S/cm².

In the compartmental model of the entire pyramidal cell, unless otherwise indicated, a proximal focal zone of Ca^{2+} electrogenesis was simulated by inserting Ca^{2+} conductance in the first 50 μm length of the apical dendrite emerging from the soma, with the following conductance parameters: $g_{Ca,max}$ = 0.007 S/cm²; $g_{K,max}$ = 0.001 S/cm²; g_{leak} = 0.0001 S/cm². The distant zone consisted of a 50-μm-long patch of apical dendrite situated 350 μm from the soma with the same parameters, except that $g_{Ca,max}$ was 0.009 S/cm².

Simulations of two Ca^{2+} channel types at the same site were done in the compartmental model, with Ca^{2+} and K^+ conductances inserted only in the soma compartment. Leak and K^+ conductances were as above. The properties of the two Ca^{2+} channels were as described above, with the exception that for one, the curve relating activation to voltage was shifted by 35 mV in the negative direction. For the standard HVA-type current, $g_{Ca,max}$ was 0.0035 S/cm²; for the other Ca current, $g_{Ca,max}$ was 0.0025 S/cm².

Measuring breakpoint. Toward the end of a simulated Ca^{2+} spike, the gradual voltage decline becomes so steady that its second derivative is nearly zero. The breakpoint, that is, the critical voltage from which the repolarization phase commences, was defined as that voltage at which the second derivative was greater than 0.02 V/sec². Breakpoint was not determined in this way for experimental data because of low-voltage, high-frequency noise. However, since the voltage decline just prior to the repolarization phase was extremely steady in most cells, breakpoint could generally be readily determined as the most depolarized point at which the voltage deviated from the slope of the plateau.

Results

Intracellular recordings were made from 61 neurons (51 from guinea pigs and 10 from rats) in neocortical slices bathed in 1 mM TTX and 24 mM TEA. All cells generated prolonged (100–1500 msec) Ca^{2+} spikes with thresholds between −40 and −30 mV. During the spike, the voltage reached an initial peak of around 0 mV and then declined gradually to a critical voltage from which a rapid repolarization phase commenced. This "breakpoint" is thus defined as the point on the plateau at which the rate of voltage decrement begins to accelerate from its previous steady and slow level (Fig. 1*A*).

In 29 cells, repolarization was associated with a prominent, prolonged depolarizing afterpotential (DAP). As previously reported (Friedman et al., 1992), this DAP, which is both Ca^{2+} and Na^+ dependent, may reflect activation of an electrogenic Na^+/Ca^{2+} exchange mechanism. The waveform of the DAP consisted of a very gradual increase and then decrease in potential, which was clearly distinguishable from the abrupt repolarization "steps" described below. Nonetheless, because the DAP obscured events during and just after the phase of spike repolarization, these neurons could not be used in the detailed analysis.

Forty-seven percent of guinea pig neurons and 90% of rat neurons showed stepwise repolarization from the plateau (Fig. 1*C,D*). That is, following the initial breakpoint and rapid repolarization, the membrane settled at one or more additional steady voltage levels, each with its own distinct breakpoint. Often, the membrane potential flipped back and forth from one step to another, indicating independent thresholds for each plateau level (Fig. 1*D*). Durations of the different steps varied from cell to cell. Breakpoint voltages also varied, but were constant for any given neuron.

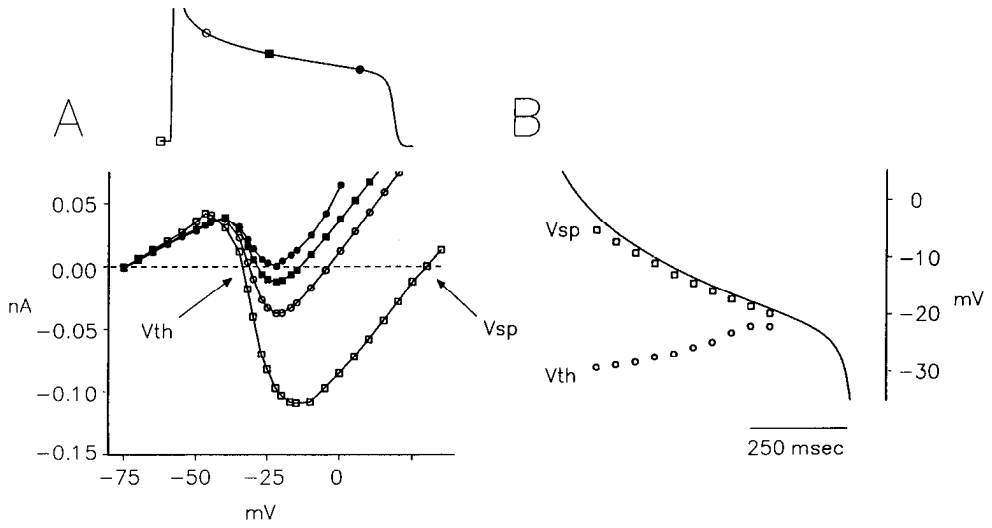

Figure 2. Current/voltage relationships before and during a Ca^{2+} spike simulated in a single-compartment computer model. *A*, Instantaneous *I/V* curves were constructed at rest (*open squares*) and at various times during the course of the simulated plateau, by switching the model from current clamp to the voltages indicated. Each *curve* shows the instantaneous *I/V* relationship at a different time during the plateau, indicated by the appropriate *symbol* on the representative Ca^{2+} spike *above*. During the plateau, there is a region of net inward current bounded by the right-hand intersection with the voltage axis (V_{sp}) and the middle intersection (V_{th}). As the plateau proceeds, these intersections approach each other. *B*, *Solid line* shows the simulated Ca^{2+} plateau, *open squares* plot the stable voltage point (V_{sp}), and *open circles* plot the threshold for all-or-none repolarization (V_{th}), as determined every 50 msec during the spike.

Factors determining the breakpoint voltage

Our understanding of the mechanisms that underlie generation of the plateau potential and its repolarization is based on early reconstructions of plateaus in TEA-exposed squid giant axons (Fitzhugh, 1960) and cardiac Purkinje fibers (Noble and Tsien, 1969). Figure 2*A* shows the instantaneous *I/V* curves that we obtained in an isopotential, single-compartment model before a Ca^{2+} plateau and at various points during its course. At the beginning of the plateau, the instantaneous *I/V* relation has a region of net inward current, between −30 mV and −5 mV, which prevents repolarization. At this time, the membrane potential is drawn toward a depolarized voltage at which net current is zero, and which, like the resting potential, lies in a region of the *I/V* curve that has a positive slope and is therefore a stable point (V_{sp}). Between these stable extremes, there is another zero current point that is unstable because it lies in a region of negative slope. This point constitutes a threshold voltage (V_{th}); if the membrane is hyperpolarized beyond this point, it will undergo all-or-none repolarization. During the course of the Ca^{2+} plateau, the instantaneous *I/V* relation changes continuously, as the Ca^{2+} current gradually inactivates and outward currents are activated. As the *I/V* curves shift in the outward direction, V_{sp} and V_{th} converge (Fig. 2*B*); eventually, they meet at the breakpoint voltage, net current becomes outward, and all-or-none repolarization commences. The point at which they converge is at the nadir of the U-shaped *I/V* curve. During the plateau, as outward currents are activated, the nadir of the U

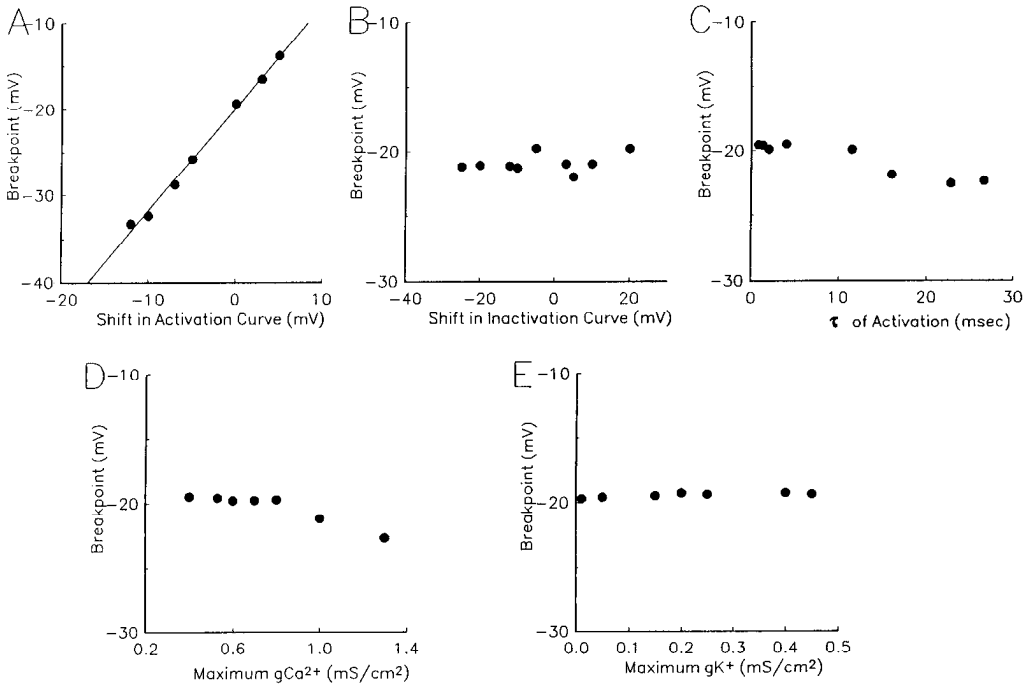

Figure 3. The effects of changing various Ca^{2+} channel parameters (*A–C*) and relative strengths of g_{Ca} and g_K (*D*, *E*) on the breakpoint voltage of a Ca^{2+} spike simulated in a single-compartment computer model. *A*, Breakpoint voltage was extremely sensitive to shifts along the voltage axis of the Ca^{2+} current/activation curve. Least-squares regression yielded a slope of 1.2. By contrast, breakpoint voltage was largely insensitive to shifts in the Ca^{2+} current/inactivation curve (*B*) and in the time constant of activation (*C*). Similarly, breakpoint voltage was not sensitive to wide changes in the maximum conductance for Ca^{2+} (*D*) or K^+ (*E*). In the former case, g_K was held constant at 0.2 mS/cm²; in the latter case, g_{Ca} was held constant at 0.535 mS/cm².

shifts along the voltage axis; however, in the presence of high TEA, this shift is minimal, and the breakpoint voltage is primarily determined by the voltage dependence of the Ca^{2+} channels.

Analysis of experimentally recorded Ca^{2+} spikes indicated that the breakpoint voltage was indeed extremely stable. Figure 1*A* shows that neither the breakpoint voltage nor the time course of fast repolarization was sensitive to variations in plateau duration and, hence, in the amount of prior intracellular Ca^{2+} concentration increase. Similarly, these parameters were the same for plateaus triggered every 10 sec and for plateaus triggered at frequencies greater than 1 Hz, despite the considerably different Ca^{2+} loading expected under these two conditions. In addition, the breakpoint was only minimally influenced by changes in the relative ionic conductances during the action potential. This is illustrated in Figure 1*B*, which shows the development of the Ca^{2+} spike during the wash-in of the TTX-TEA bathing medium. As the Na^+ current blocked and the initial, fast spike disappeared, the maximum initial amplitude of the remaining spike shifted by 12 mV to a more depolarized level. Meanwhile, as K^+ current blocked, the action potential also became more prolonged and the AHP disappeared. Yet, despite these significant changes in the relative contribution of Ca^{2+} conductance to the net current, the breakpoint voltage varied by no more than 5 mV.

The breakpoint voltage was similarly constant in computer simulations of calcium spikes under different initial conditions of relative Ca^{2+} and K^+ conductance, which were performed in a single-compartment (isopotential) model. Figure 3 shows the effect on the breakpoint of systematically varying properties of the Ca^{2+} channels, including voltage dependence of activation (*A*) and inactivation (*B*) and time constant of activation (*C*). Figure 3, *D* and *E*, shows the effect of varying the densities of the Ca^{2+} conductance and the K^+ conductance, respectively. It can be seen that while the breakpoint voltage was largely insensitive to all of these parameters, it was extremely sensitive to slight shifts in the voltage/activation curve. Thus, a least-square fit to the data in Figure 3*A* yielded a slope of nearly 1, indicating that the breakpoint voltage is directly determined by the curve relating current activation to membrane potential.

The strong correlation between the value of the breakpoint and the voltage dependence of the underlying Ca^{2+} current was experimentally demonstrated by substituting Ba^{2+} for Ca^{2+} in the bathing medium. Figure 4 shows that Ba^{2+}, which is known to cause a hyperpolarizing shift in the voltage/activation curve of the HVA Ca^{2+} channel by about 10 mV (Wilson et al., 1983; Huguenard and Prince, 1992), caused the breakpoint to shift in the hyperpolarizing direction by 8 mV. The Ca^{2+} plateau also became markedly prolonged, as expected from the actions of Ba^{2+} on K^+ channel blockade (Krnjevic et al., 1971) and Ca^{2+} channel inactivation (Gutnick et al., 1989). However, these latter effects were probably not related to the shift in the breakpoint. Thus, Figure 1*B* shows that breakpoint did not become more hyperpolarized when spike broadening was due to TEA-induced K^+ channel blockade. Moreover, Friedman and Gutnick (1989) showed that when, in the presence of TTX and TEA, additional spike prolongation was induced by intracellular injection of a Ca^{2+} chelator, it was not associated with a shift in breakpoint.

In summary, although the breakpoint is somewhat sensitive to a variety of influences, it is most dependent on the voltage/activation relationship of the Ca^{2+} current. Here, it corresponds

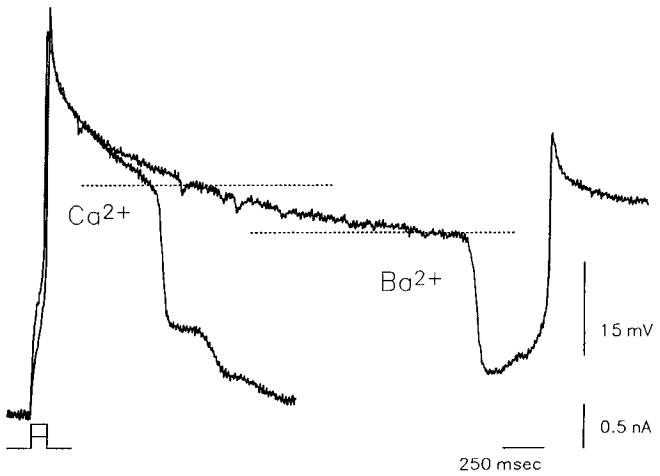

Figure 4. Effect of replacing extracellular Ca^{2+} with an equimolar concentration of Ba^{2+}. Superimposed are a Ca^{2+} spike and a Ba^{2+} spike from the same neuron. Note that substitution with Ba^{2+} caused extreme prolongation of the plateau, and a hyperpolarizing shift in breakpoint voltage (*dashed line*) by 8 mV.

to voltages in a narrow region on the shoulder of the curve, near maximal activation, since deactivation of the Ca^{2+} current becomes regenerative at less positive potential levels. In the present experiments, breakpoints of the largest plateaus ranged between −30 mV and +8 mV (15.1 ± 6.1, mean ± SD; $n = 40$), which is in good agreement with parameters estimated for the HVA channel in the neocortex on the basis of voltage-clamp data (Sayer et al., 1990).

Models of stepwise repolarization

Two distinct hypotheses might account for the stepwise repolarization of Ca^{2+} spikes in neocortical neurons; each was simulated by a different computer model.

Model 1. Multiple plateau levels might reflect multiple sites of calcium electrogenesis that are electrotonically separated by intervening regions in which spike propagation is passive. Thus, the larger plateaus would reflect a proximally generated Ca^{2+} spike, while the lower-voltage steps would reflect Ca^{2+} spikes generated distally in the dendrites. This hypothesis was simulated with a multicompartmental model, as shown in Figure 5*A*. In this model, the voltage recorded in the soma at each breakpoint reflects the voltage dependence of the Ca^{2+} channels involved, and the distances of the distinct sites of spike initiation from the recording electrode.

Model 2. Two plateau levels might reflect the presence of two populations of Ca^{2+} channels with voltage/activation curves located at different points along the voltage axis. Each step would then be associated with one of the channels, since each would confer a unique threshold for repolarization. This hypothesis was simulated by inserting two types of Ca^{2+} channels only at the soma and leaving the entire dendritic tree passive. As illustrated in Figure 5*B*, in this model the voltage at each breakpoint is a manifestation of the voltage-dependent properties of a particular type of Ca^{2+} channel.

Effects of brief hyperpolarizing pulses

We reasoned that a hyperpolarizing pulse applied during the Ca^{2+} plateau would more readily achieve repolarization threshold at a proximal electrogenic site than at a distal one. Figure

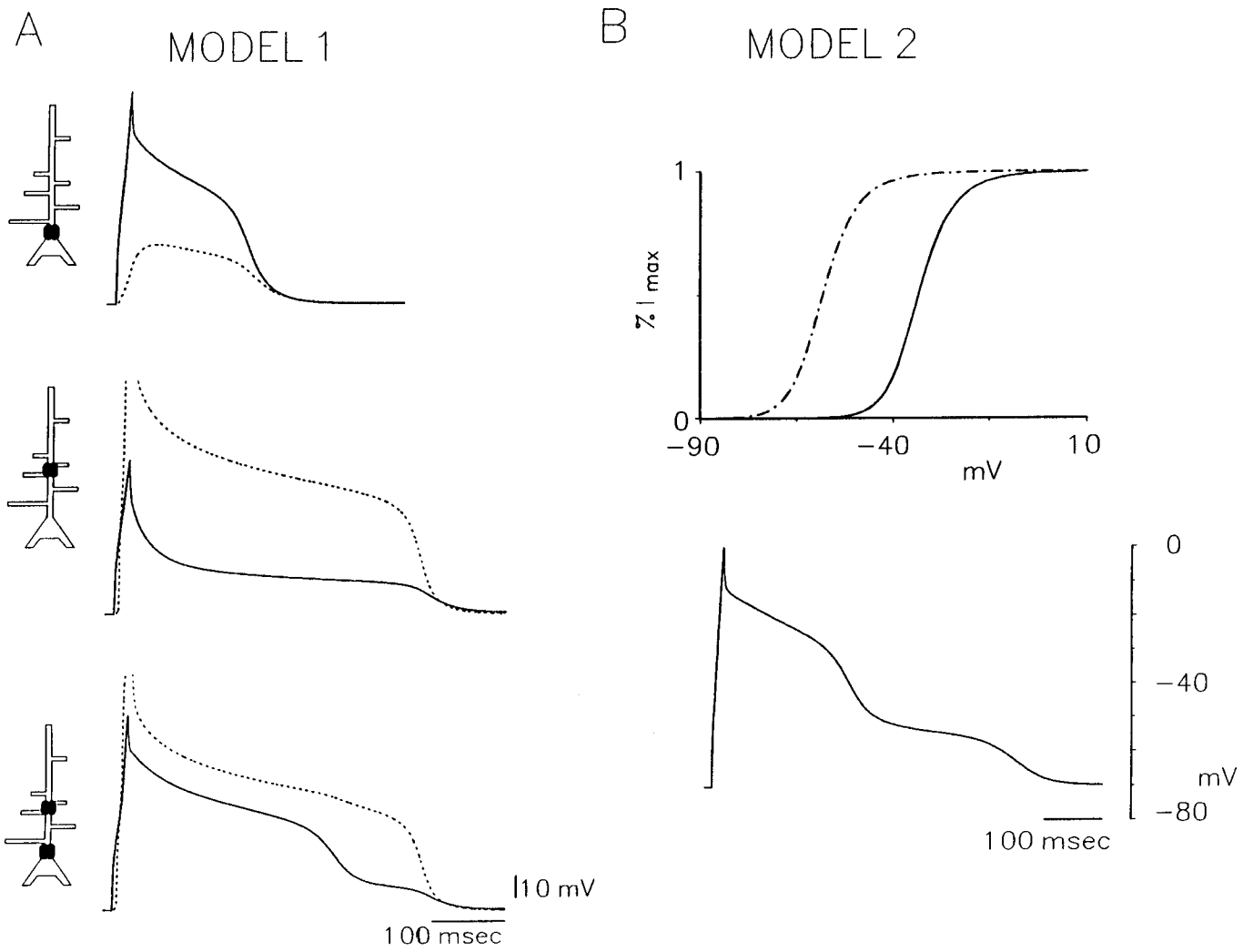

Figure 5. The phenomenon of stepwise repolarization was simulated in the computer by two distinct models. *A*, In model 1, Ca^{2+} channels with identical characteristics were inserted either in one proximal dendritic compartment immediately adjacent to the soma (*upper traces*), in one more distal dendritic compartment 350 μM from the soma (*middle traces*), or in both compartments (*lower traces*). In each set of superimposed traces, the *solid line* shows the somatic recording and the *dashed line* shows the dendritic recording during a Ca^{2+} spike triggered by a brief intracellular current pulse. In the *diagrams, thickened lines* indicate the approximate relative location of Ca^{2+} channels. *B*, In model 2, g_{Ca} was confined to the soma compartment, where two different Ca^{2+} channel types, with different voltage/activation characteristics, were inserted. *Upper curves*, Voltage/activation relationships for the two channel types. *Lower trace*, Somatic Ca^{2+} spike evoked by a brief intracellular depolarizing pulse. Note that this model yields a stepwise repolarization phase in which each breakpoint voltage corresponds to the shoulder of one of the Ca^{2+} activation curves.

6, *A* and *B*, shows that imposing a brief (10–20 msec) pulse of hyperpolarization caused the large plateau to terminate abruptly. The step persisted, however; indeed, in some cases, several additional steps that had previously been masked by the large plateau were revealed in this way (Fig. 6*B*). Whenever they were applied, brief hyperpolarizing pulses always readily reached threshold for repolarization of the large plateau, whereas even with currents greater than 2 nA, we were never able to terminate the smaller voltage steps in this way.

As illustrated in Figure 7*A*, these data were readily simulated in the multicompartmental model with electrotonically separated sites of spike generation. In this model, large, brief pulses delivered at the soma were generally unable to affect spikes generated distally because of the low-pass filtering characteristics of the cable.

Figure 7*B* shows that it was also possible to mimic this result in the single-compartment model with two Ca^{2+} channels. In this case, however, simulation of the experimental data was far less robust. Since brief pulses supplied the same voltage change to the mechanisms responsible for both plateau levels, only over a very narrow range of pulse intensities was it possible to terminate the large spike while leaving the subsequent step.

Effects of prolonged current injection

We could unambiguously distinguish between the two models by studying the effect of prolonged depolarizing and hyperpolarizing current pulses on the breakpoints of the large plateau and subsequent step, respectively. In all cells tested ($n = 6$), the breakpoint voltage of the large plateau was almost uninfluenced by the current injection, whereas that of the subsequent step was shifted in the depolarizing or hyperpolarizing direction (Fig. 8*A*). This is shown graphically by the circles in Figure 8*B*, which plots the breakpoint voltages for one cell as a function of membrane potential before the spike. A least-squares regression re-

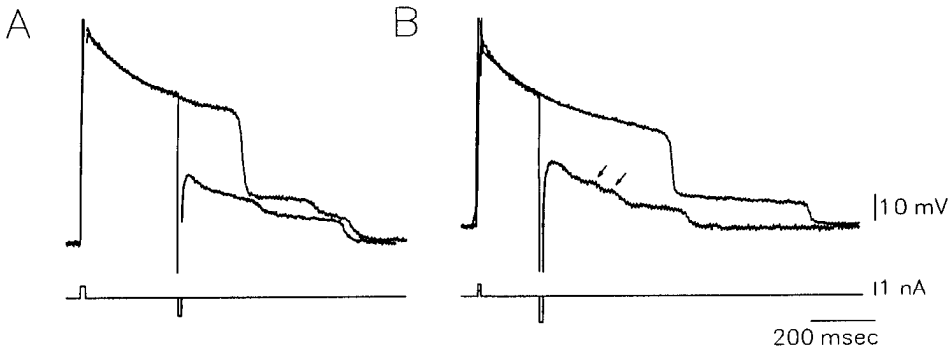

Figure 6. Effect of brief hyperpolarizing pulses on repolarization from the Ca^{2+} plateau. Brief (20 msec), intense (>1 nA) hyperpolarizing current pulses, applied during the Ca^{2+} spike, caused repolarization from the largest plateau without terminating the lower-amplitude plateau levels. Often, additional plateau levels were uncovered in this way (*B, arrows*). Traces in *A* and *B* are from the same neuron.

vealed a very slight positive slope for this relationship for the large plateau and a steep slope for the smaller step.

Also shown on this graph are the results of computer simulation of this experiment in the two models. In both cases, the breakpoint of the large plateau was almost unaffected by prolonged somatic current injection. This similarity to the experimental data persisted in the multicompartmental model with electrotonically separated sites of spike generation: the breakpoint voltage of the smaller step varied steeply as a linear function of the resting membrane potential imposed by the injected current. By contrast, in the single-compartment model with two Ca^{2+} channels, the breakpoint of the smaller step was not affected by the current.

It is thus apparent that the Ca^{2+} spike that gave rise to the smaller plateau arose at a point electrotonically distant from the site of current injection; it propagated passively to the soma, where it summed with the local voltage change imposed by the injected current. We consistently observed a slight positive slope in the relationship for the larger plateau, which may indicate that this Ca^{2+} spike, too, was generated at a site somewhat distant to the point of electrode penetration, albeit more proximal than that which gave rise to the step.

Rate of repolarization

During repolarization, the transition of the membrane potential from the breakpoint to the next plateau level (or to the resting potential) followed a complex time course. Although this time course varied somewhat from cell to cell, in all cases the potential change had achieved its maximum velocity by the time it reached 75% of the interstep voltage, and did not begin to decelerate until it reached 25%. Thus, in the middle 50%, the potential fell at constant velocity and could be readily fit to a straight line. In general, this highest rate of repolarization, a, was slower the lower the voltage of the previous breakpoint. For the largest plateaus, a was 0.59 ± 0.26 V/sec ($n = 12$). This is about three times slower than what would be expected of a process whose rate was determined by the membrane time constant.

Figure 9*A* summarizes pooled data from seven neurons in which the ratio of the sizes of the two plateaus at the breakpoint (V_2:V_1) was plotted as a function of the ratio of the subsequent maximal rates of repolarization (a_2:a_1). This plot yielded a straight line ($r^2 = 0.97$) with a slope of 1, demonstrating that the two ratios were equal. This finding is consistent with electrotonic decrement of an identical waveform initiated at different distances from the recording site (see Discussion).

Computer simulations were used to aid in estimating the sensitivity of this measure to small differences in the waveform at the two sites of Ca^{2+} electrogenesis, as follows. Clusters of Ca^{2+} channels were inserted at two foci along the apical dendrite, and the breakpoint voltage at the distant site was changed systematically by shifting the activation curve of the channel along the voltage axis (see Fig. 3*A*). The distance between the two sites was changed, and V_2:V_1 was plotted against a_2:a_1, as above. When the distal and proximal channel types were the same, the relationship was linear with a slope of 1 and $r^2 = 0.99$. For each

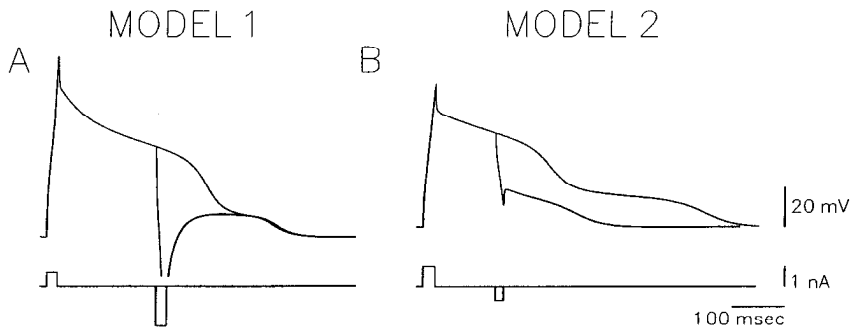

Figure 7. Computer simulation of the effect of brief hyperpolarizing pulses. In *A* and *B*, model 1 and model 2 are as in Figure 5. In both models, brief hyperpolarizing pulses were able to cause repolarization from the largest plateau without terminating the lower-amplitude plateau. However, in *model 2*, in which Ca^{2+} channels with different voltage dependencies were inserted into one somatic compartment, termination of both plateau levels could only be prevented if the current pulse was smaller than 0.7 nA. By contrast, in *model 1*, in which identical Ca^{2+} channels were inserted into spatially separated compartments, the simulation was much closer to the experimental result; somatically applied hyperpolarizing pulses greater than 2 nA were not able to trigger repolarization from the lower-amplitude plateau.

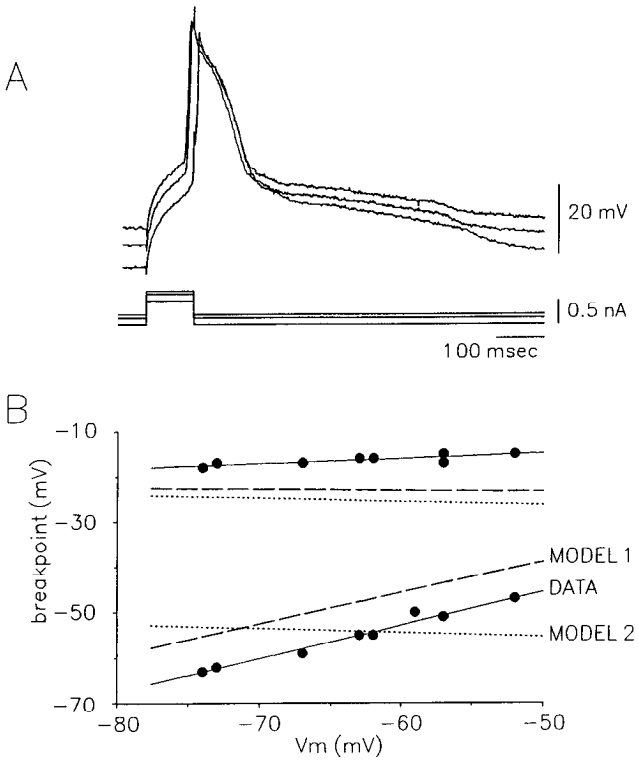

Figure 8. Effect of continuously injected current on the breakpoint voltages of the high-amplitude and low-amplitude plateaus. *A*, Superimposed traces of Ca^{2+} spike at resting potential and during injection of depolarizing and hyperpolarizing currents. Note that DC current did not affect the breakpoint voltage of the high-amplitude plateau, but did deflect the breakpoint voltage of the lower-amplitude plateau. *B, Solid circles* plot the experimentally determined breakpoint voltages of the high-amplitude plateau (*upper points*) and the lower-amplitude plateau (*lower points*), as a function of the pre-Ca^{2+} spike membrane potential level during the DC current injection. *Solid line* is a linear regression line fitted to the experimental data; *dashed line*, simulation of this experiment with model 1; *dotted line*, simulation of this experiment with model 2. Note that the experimental results could only be successfully simulated with *model 1*, in which identical Ca^{2+} channels were inserted into spatially separated compartments. Model 1 and model 2 are as in Figure 5.

case in which the distant channel, and hence the breakpoint amplitude of the distant plateau, differed from that of the proximal one, the relationship was clearly linear, but with a slope significantly other than 1. In Figure 9*B*, which plots the r^2 values obtained by testing the goodness of fit of these curves to the experimental data, it can be seen that only identical Ca^{2+} channel characteristics in the two compartments yielded a correlation coefficient greater than 0.95.

Distribution of electrogenic zones

The above findings lead us to conclude that breakpoint voltage is the same at each site of spike generation, as is the repolarization rate. Therefore, V_2:V_1 is related to the ratio of electrotonic distances between the active zones and the recording site. If two active zones and the recording site are distributed serially along a single cable, and both electrogenic regions are on the same side of the recording site, the V_2:V_1 ratio is a direct function of the electrotonic distance between them. Obviously, if the active zones are very close to each other, they will not operate independently but will effectively constitute a single zone, and stepwise spike repolarization will not be observed. Figure 10 shows computer simulations in which the electrotonic distance between the active zones was varied. In this example, stepwise repolarization was only seen if the interzone distance was greater than $0.65L$, where L is the electrotonic distance of the core conductor (Rall, 1977), in which case the V_2:V_1 ratio was 0.52. Although the minimum distance did vary somewhat with differing current densities and membrane properties, in all trials, stepwise repolarization was never seen when the distance between clusters of Ca^{2+} channels was less than $0.48L$, and the V_2:V_1 ratio was greater than 0.62. Yet, much higher ratios were often encountered experimentally, as can be seen in the histogram of Figure 11. These results could be simulated in the computer model either by inserting the Ca^{2+} channels in the dendritic branches but not in the main apical dendrite (Fig. 12*A*), or by creating one active zone in the apical dendrites and another in the basal tree, such that the recording site was between them (Fig. 12*B*).

In all the computer simulations presented above, active zones of Ca^{2+} electrogenesis were modeled as "hot spots," created by focally inserting Ca^{2+} conductance along a restricted dendritic region. For example, in the simulation illustrated in Figure 12*C*, stepwise repolarization occurred when Ca^{2+} conductance was inserted at two locations: along the first 50 μm segment of the apical dendrite and along a 50 μm segment located 350 μm from the soma. Figure 12*D* shows the result obtained when the distant active zone was created by adding Ca^{2+} conductance, with the same density, throughout the entire distal dendritic tree, from 350 μm and beyond. The smaller plateau was considerably prolonged under the latter conditions, but the breakpoint voltage was the same for both. Both of these curves are entirely consistent with the experimental data obtained in different cells.

Discussion

Neocortical neurons contain a wide assortment of conductances to various ions. These have different voltage-dependent properties and are probably distributed unevenly throughout the soma–dendritic membrane. Our strategy for studying the distribution of HVA currents has been to block other conductances. Voltage-dependent Na^+ currents in neocortical neurons are essentially completely blocked at this concentration of TTX . Although some slow K^+ conductance may be resistant to moderate doses of TEA (Schwindt et al., 1988a), the absence of a prominent AHP shows that the K^+ current was minimal with the large dose we used. Nonetheless, some persistent K^+ conductance probably contributed to the slope of the Ca^{2+} plateau as it declined to the breakpoint voltage, although Ca^{2+}-dependent inactivation of Ca^{2+} current undoubtedly also played a role in this decline. Thus, Friedman and Gutnick (1989) showed that under these experimental conditions, the Ca^{2+} plateau is greatly prolonged by intracellular injection of a Ca^{2+} chelator. As to which type of Ca^{2+} channel might be involved, a prominent T-type current has been reported in neocortex (Friedman and Gutnick, 1987; Sutor and Zieglgansberger, 1987; Sayer et al., 1990) and indeed its presence in dendrites has been hypothesized (Friedman and Gutnick, 1987). However, the Ca^{2+} plateaus studied here were so prolonged as to ensure complete inactivation of this transient conductance (Friedman and Gutnick, 1987; Sutor and Zieglgansberger, 1987; Sayer et al., 1990). Our data do not allow us to distinguish between N-, L-, and P-type HVA channels (Tsien et al., 1988; Llinas et al., 1989; Sayer et al., 1990), since each of these can mediate a sustained current and we did not use pharmacological blockers.

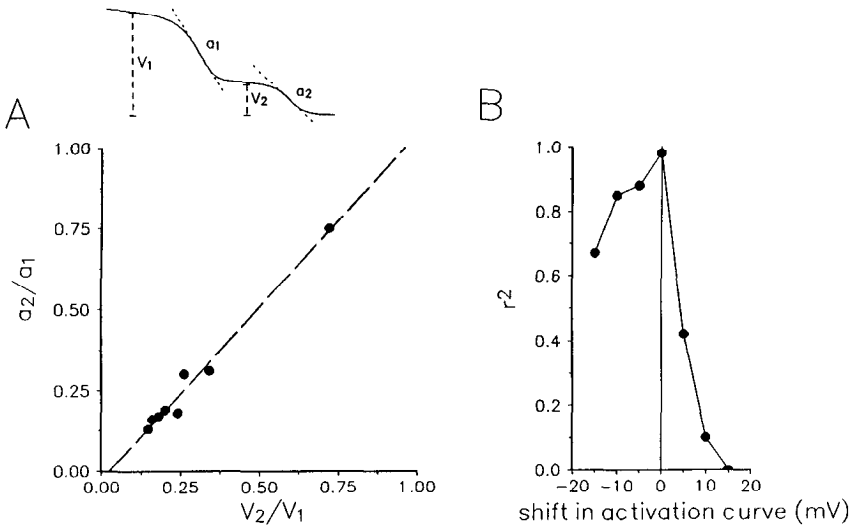

Figure 9. Ratio of breakpoint voltages of the plateau levels (V_2:V_1) equals the ratio of the maximal rates of repolarization from those levels (a_2:a_1). *A*, Plot of a_2:a_1 versus V_2:V_1, measured for seven different experiments as in *diagram*, fits a 45° line (*dashed line*) with $r^2 > 0.97$. All measurements were made in the absence of background DC current injection. *B*, In computer simulations of Ca^{2+} spikes generated by model 1, the experimentally observed equality of the voltage and repolarization rate ratios could only be achieved when both proximal and distant Ca^{2+} channels had identical voltage-dependent characteristics. The voltage/activation curve of the distal Ca^{2+} conductance was systematically shifted, for each channel type the distance between the two sites of Ca^{2+} channel insertion was systematically changed, and the resultant voltage and repolarization rate ratios were fitted to a straight line. The r^2 values, obtained by testing the goodness of fit of this regression line to the experimental data, are plotted as a function of the shift of the activation curve of the distal Ca^{2+} channel along the voltage axis.

Confirmation of the multicompartmental model

Our analysis indicates that the stepwise repolarization of Ca^{2+} spikes, which we observed in more than 50% of neocortical neurons exposed to TEA and TTX, was a reflection of several sites of Ca^{2+} electrogenesis separated by intervening, electrotonically separated regions through which propagation was passive. In computer simulations, the alternative explanation—multiple types of Ca^{2+} channels evenly distributed but with different voltage sensitivities—could also produce stepwise repolarization. However, only the model that entailed a nonhomogeneous distribution of electrogenic sites could simulate the observed effect of prolonged current pulses on breakpoint voltage and the inability of very large hyperpolarizing pulses to terminate the small plateaus.

It seems likely that our analysis would be applicable to other CNS areas where stepwise repolarization of Ca^{2+} spikes has been observed under similar experimental conditions. Llinas and Yarom (1981) reported two plateau levels in inferior olive neurons,

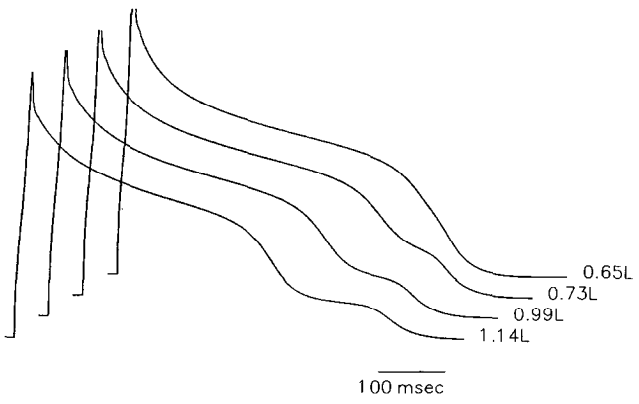

Figure 10. In computer simulations with model 1, the electrotonic distance between the proximal and the distal site of Ca^{2+} electrogenesis was systematically changed in order to determine the minimal distance at which stepwise repolarization could still be generated. Distance is expressed in units of electrotonic length (L). For these simulations, the Ca^{2+} conductance density was 0.009 S/cm² in the proximal compartment and 0.011 S/cm² in the distal compartment. Note that in this stimulation, stepwise repolarization was not obtained when the spatial interval was 0.65L or smaller.

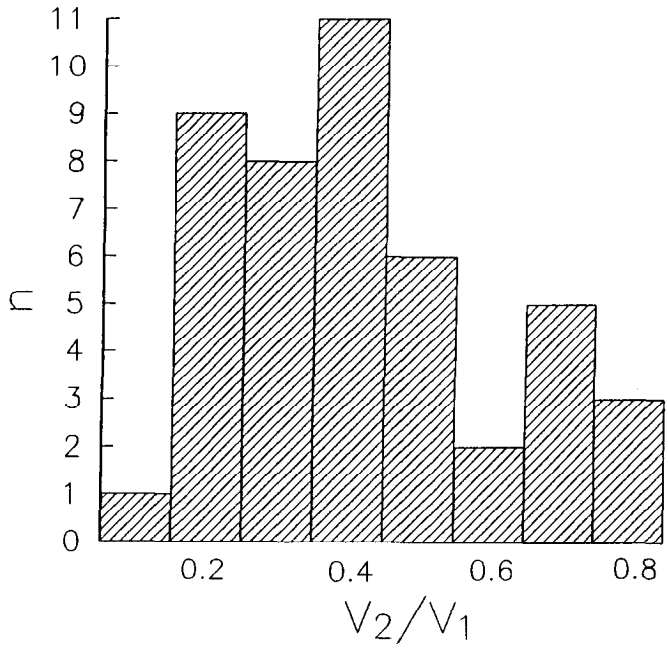

Figure 11. Histogram showing the distribution of experimentally observed V_2:V_1 ratios for 34 neurons. In each case, V_1 was the breakpoint voltage of the highest-amplitude plateau.

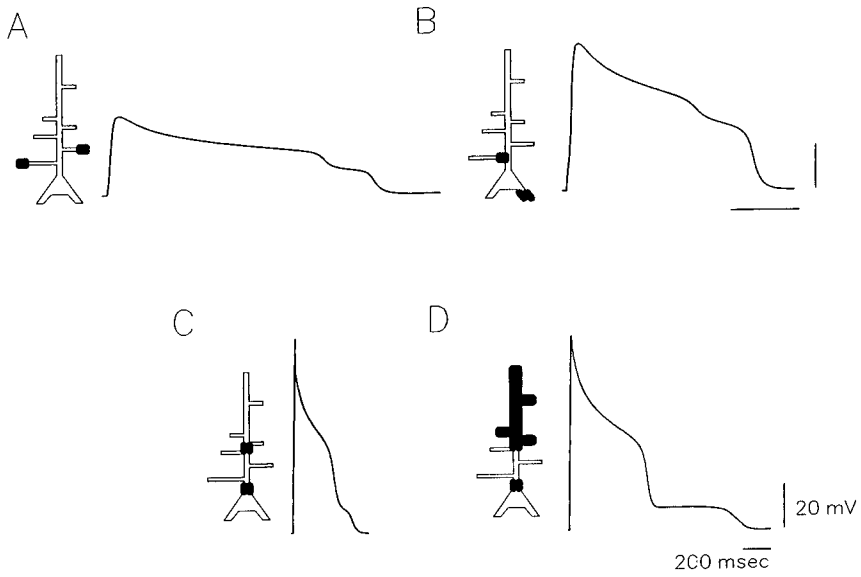

Figure 12. Computer simulations to demonstrate the effect of changing the spatial distribution of electrotonically separated clusters of Ca^{2+} channels. *A* and *B*, Very high V_2:V_1 ratios can be obtained when Ca^{2+} channels are restricted to compartments located in the distal tips of different dendritic branches (*A*), or when they are inserted on different sides of the recording site, as in an apical dendritic compartment and a basal dendritic compartment (*B*). In the *diagrams, thickened lines* indicate the approximate relative location of Ca^{2+} channels. *C*, Ca^{2+} channels restricted to two, electrotonically separated compartments that are both situated in the main stem apical dendrite. *D*, The dendritic area that is free of active Ca^{2+} electrogenesis is the same as in *C*, but Ca^{2+} channels have been inserted into all distal dendritic compartments.

as did Leonard and Wickelgren (1985) in mechanosensory neurons of lamprey spinal cord. In both these studies, the smaller plateau levels were ascribed to Ca^{2+} electrogenesis at electrotonically distant sites.

Similarity of the Ca^{2+} spike waveform in all compartments

Crucial to our analysis is the fact that although a variety of influences may slightly modify the breakpoint voltage, it depends primarily on the curve relating Ca^{2+} channel activation to membrane potential, where it corresponds to the voltage range just under maximal activation. Thus, replacement of Ca^{2+} with Ba^{2+}, which shifts this curve to the left, was associated with an appropriate shift in breakpoint amplitude. Moreover, as seen both in computer simulations (Fig. 3*C,D*) and experimentally, as blockers of Na^+ and K^+ currents took effect (Fig. 1*B*), breakpoint voltage was largely insensitive to changes in the relative Ca^{2+} and K^+ conductances. We are therefore able draw conclusions about the characteristics of the responsible Ca^{2+} channel on the basis of the observed breakpoint voltage. Our finding that breakpoint of the large plateau was around −15 mV is consistent with the report by Sayer et al. (1990) that peak Ca^{2+} current in neocortical neurons is generated in the range of −10 to −20 mV.

One remarkable finding was that the ratio of breakpoint voltages was equal to the ratio of maximum repolarization rates. For an infinite cable, this is the relationship we would predict for electrotonic propagation of an identical waveform from distant active sites. Hodgkin and Rushton (1946) showed that when a steady state voltage, which is analogous to the plateau voltage V_1 at the breakpoint, is generated at one point along an infinite cable, the voltage recorded at a different point (V_2) is related to L as follows:

$$V_2 = V_1 \cdot \exp(-L), \quad V_2/V_1 = \exp(-L)$$

Similarly, it can be shown (see Appendix) that when a linearly changing current is applied at one point on an infinite cable, where it creates a voltage change analogous to the linear slope of repolarization, a_1, the slope of the voltage change recorded at a different point (a_2) is related to L as follows:

$$a_2 = a_1 \cdot \exp(-L), \quad a_2/a_1 = \exp(-L).$$

Of course, an infinite cable hardly describes the morphological complexity of a neocortical neuron, either as recorded experimentally or as simulated in our compartmental model. Although we have not made calculations for the actual boundary conditions that prevail in these cells, results of our computer simulations show that the relationship between voltage, rate of repolarization, and electrotonic distance remains robust in a closed-ended, branching dendritic tree.

Thus, our experimental observation that $V_2/V_1 = a_2/a_1$ constitutes strong evidence that the distant Ca^{2+} spike is identical to the proximal one, at least in terms of breakpoint voltage and kinetics of repolarization. In view of the close relationship between Ca^{2+} channel characteristics and Ca^{2+} spike waveform, we conclude that the HVA channels at all electroresponsive sites have the same voltage/activation relationship. The conclusion is in good agreement with the recent report (Brown et al., 1992) that although the HVA current of neocortical neurons consists of pharmacologically distinct components, all have the same kinetic and voltage-dependent properties.

Dendritic location of distant Ca^{2+} electrogenesis

Our analysis is neutral on the question of precisely where the distant Ca^{2+} spike is generated. The most plausible location is the distal dendrites. This would fit evidence that TTX-resistant active responses can be elicited in neocortical dendrites (Stafstrom et al., 1985; Amitai et al., 1993), and imaging data from a variety of brain regions indicating a dendritic site of Ca^{2+} entry through voltage-dependent channels. However, since dye coupling between neurons has been clearly demonstrated in neocortical slices (Gutnick and Prince, 1981; Connors et al., 1984; Gutnick et al., 1985), we cannot rigorously rule out the possibility that the small steps reflect Ca^{2+} spike generation in adjacent, electrotonically coupled cells. This explanation seems unlikely, however; in our experience, incidence of stepwise repolarization was higher in rats than in guinea pigs, whereas incidence of dye coupling has been shown to be much lower in mature rats (Connors et al., 1984).

It has been suggested that in a geometrically inhomogeneous structure, focal patches of heightened electrical excitability might exist despite uniform active membrane properties. In a strongly branching dendritic system, these "hot spots" would be located

at sites of dendritic bifurcation, where current density per unit area of membrane would be enhanced (Lorente de No and Condouris, 1959; Llinas and Nicholson, 1971; Dimitrova and Dimitrov, 1991). In an attempt to test whether this might be the case in the present study, we performed a series of computer experiments using a very large compartmental model to simulate accurately the elaborate dendritic tree. We tried a wide range of membrane parameters and relative ionic conductances, but were unable to replicate stepwise repolarization of the Ca^{2+} spike if the Ca^{2+} conductance was inserted uniformly throughout the neuronal membrane. This negative result, along with growing evidence for nonhomogeneous dendritic distribution of Ca^{2+} channels in various brain regions, leads us to consider it more likely that in neocortical pyramidal cells, the patches of enhanced Ca^{2+} electrogenesis reflect "hot spots" of increased Ca^{2+} channel density.

Electrophysiological evidence of high-threshold dendritic Ca^{2+} spikes has been reported for a variety of central neurons, including cerebellar Purkinje cells (Llinas and Nicholson, 1971; Llinas and Sugimori, 1980; Ross and Werman, 1987; Ross et al., 1990; Sugimori and Llinas, 1990), hippocampal pyramidal cells (Wong et al., 1978; Masukawa and Prince, 1984; Jaffe et al., 1992), inferior olivary cells (Llinas and Yarom, 1981), and thalamic relay cells (Jahnsen and Llinas, 1984). Voltage-clamp studies of Stafstrom et al. (1985) suggested that in cat neocortical cells, the dendritic tree is the primary site of active Ca^{2+} conductance. Consistent with this is our recent observation of relatively prolonged, TTX-insensitive spikes in intradendritic recordings from guinea pig neocortical pyramidal neurons (Amitai et al., 1993).

Distribution of HVA Ca^{2+} channels in neocortical dendrites

Although our data do not specify the precise location of the dendritic Ca^{2+} channels, they do provide some strong clues. Our findings indicate that there are at least two regions on the cell membrane with a relatively high density of Ca^{2+} channels, and that these are separated by a large area in which the Ca^{2+} conductance either is not present at all, or is too low to generate a spike even under these extreme conditions of K^+ current blockade. The apical stem dendrite, which is a long and relatively thin cable, is most likely to be the region scarce in Ca^{2+} channels; however, this region might extend to include the basal dendritic stems and the somatic membrane as well.

It is possible that the more proximal electrogenic region, which is responsible for the high-amplitude plateau, is located in the somatic membrane. Indeed, Westenbroek et al. (1990) recently reported that in hippocampal pyramidal cells, L-type Ca^{2+} channels, visualized using a monoclonal antibody, are clustered in the cell body and at the base of major dendrites. However, our finding that in some cells the breakpoint of the largest plateau was somewhat shifted by prolonged current injections (Fig. 8) argues for a nearby dendritic location. The basal dendrites of neocortical pyramidal cells can be extremely elaborate and complex, yet since the main basal dendritic stems are relatively short, they may begin to branch at points that are electrotonically close to the soma. Thus, although we have not explored this in the present study, we consider it feasible that what constitutes a "proximal" site from an electrotonic viewpoint might in fact reflect Ca^{2+} electrogenesis in the basal dendritic system. In this event, we would expect HVA Ca^{2+} channels to be sparse or absent in the somatic and main stem dendritic membranes of neocortical neurons, as has been implied from Ca^{2+} for cerebellar Purkinje cells (Sugimori and Llinas, 1990; Lev-Ram et al., 1992) and hippocampal pyramidal cells (Jaffe et al., 1992).

As to the remote sites of Ca^{2+} electrogenesis, at the extremes one might consider isolated distal patches of high Ca^{2+} channel density on the one hand, and broad regions of uniform density encompassing much of the distal dendritic tree on the other hand. The simulations illustrated in Figure 12, *C* and *D*, show that many of our recordings could be consistent with both of these possibilities. However, the frequent occurrence of several low-amplitude steps with V_2:V_1 ratios greater than 0.7, as in Figure 5, points to independent spike generation in secondary or even tertiary dendritic branches rather than serial distribution of patches along the main dendritic stem (see Fig. 12*A*). In cultured hippocampal neurons, ω-conotoxin binding suggested that voltage-dependent Ca^{2+} channels in the dendrites are segregated into punctate clusters with intervening bare regions (Jones et al., 1989). Similarly, Westenbroek et al. (1992) found a patchy distribution of antibody-labeled N-type channels in neocortical dendrites. However, these potential "hot spots" appear to be too close to each other to account for stepwise repolarization of Ca^{2+} spikes. Moreover, because N-type channels tend to inactivate rapidly during prolonged depolarization (see Tsien et al., 1988), their presence might not be manifest as prolonged Ca^{2+} plateaus. In the study of cultured neurons, Jones et al. (1989) found that in innervated cells the Ca^{2+} channels are clustered near synaptic sites. A similar finding was reported for the dendrites of cerebellar Purkinje cells (Hillman et al., 1991), where immunohistochemical localization with an antibody to funnel-web spider toxin indicated that P-type Ca^{2+} channels are localized in spiny branchlets and on spines, as well as at sites of dendritic bifurcation. In agreement with this, several imaging studies in cerebellar Purkinje cells using Ca^{2+}-sensitive dyes (Ross and Werman, 1987; Tank et al., 1988; Ross et al., 1990; Sugimori and Llinas, 1990) show that voltage-dependent Ca^{2+} entry can occur anywhere in the distal dendritic tree, and that individual dendritic branches may be activated independently of one another.

Functional implications

Ca^{2+}-mediated action potentials have generally only been seen in somatic recordings from normal neocortical cells under conditions such as those we employed, in which rectifying K^+ currents were blocked (Connors et al., 1982; Stafstrom et al., 1984). Apparently, generation of full-blown spikes is not normally a function of the more proximal site of active Ca^{2+} electrogenesis. However, Ca^{2+} channel activation at this site may play a role in afterpotential generation and determination of firing pattern. Some DAPs in these cells are sensitive to Ca^{2+} blockers (Connors et al., 1982; Friedman and Gutnick, 1989). Moreover, several of the many K^+ currents in neocortical neurons are Ca^{2+} dependent (Schwindt et al., 1988a,b), and Friedman and Gutnick (1989) showed that intracellular injection of a Ca^{2+} chelator blocks the consequent AHPs and thereby causes a regular spiking firing pattern to be replaced by one of intrinsic bursting.

A variety of functions may be proposed for voltage-dependent Ca^{2+} channels in the distal dendrites. The most straightforward is amplification of synaptic potentials, since, in neocortex, these may be generated at a very great distance from the soma. For example, Cauller and Connors (1992) showed that activation of layer 1 input to layer 5 neurons produces somatic EPSPs that are far too large to be accounted for by passive dendritic membrane properties. In the present study, many cells showed step-

wise Ca^{2+} spike repolarization with very small V_2:V_1 ratios, suggesting that the distant electrogenic zones might be located very far out on dendritic branches, where input resistance is highest and distal synaptic input would be most effective. Indeed, in anatomically verified intradendritic recordings from neocortical pyramidal cells, K^+ blockers were not required in order to evoke Ca^{2+} spikes with intracellular current pulses (Amitai et al., 1993).

Because we used TTX, we cannot say whether voltage-dependent Na^+ channels are present in the dendrite. If they are, they probably play an important role in dendrosomatic interaction. In a recent report, Jaffe et al. (1992) elegantly demonstrated interaction of the two cationic currents in the apical dendrites of hippocampal pyramidal cells. With the use of Na^+- and Ca^{2+}-sensitive dyes, they showed that during somatic depolarization, the spatial distribution of dendritic Ca^{2+} entry depended on active invasion of Na^+ spikes into the dendrites.

In addition to an effect on the electrical integrative properties of the cell, dendritic voltage-dependent Ca^{2+} channels will have other important functional consequences related to activity-dependent regulation of Ca^{2+} entry and intracellular Ca^{2+} concentration. Ca^{2+} ions mediate a large number of cellular processes. Many of these, such as activation of ionic channels and modulation of synaptic plasticity, are extremely localized within the membrane. Where it has been studied, intradendritic diffusion of Ca^{2+} has been shown to be highly restricted (McBurney and Neering, 1987; Swanson, 1989). Therefore, the precise location of the dendritic Ca^{2+} channels must be a critical factor in determining their functional role in normal processes and in cytotoxicity (Wilson et al., 1983). In the present study, intrasomatic recordings have provided strong evidence that in neocortical neurons, as in cerebellar Purkinje cells (Tank et al., 1988; Ross et al., 1990; Sugimori and Llinas, 1990), the distal dendrites have Ca^{2+}-dependent electroresponsive properties. Whether this similarity extends to a localization of Ca^{2+} channels near sites of synaptic input has yet to be illuminated by other techniques.

Appendix

In general, the response of a linear, infinite cable to any time course of current injection $I(T)$ may be obtained from the convolution of $I(T)$ with the delta function response (Jack and Redman, 1971):

$$V(L, T) = C_0 \int_0^\infty \frac{I(T-t)}{\sqrt{t}} e^{(-L^2-4t^2)/4t}\, dt, \qquad (1)$$

where $C_0 = Q_0/(2c_m\lambda\sqrt{\pi})$ and Q_0 is the charge applied instantaneously to the cable.

In the present case, we wish to evaluate the voltage at different points along the cable in response to injection of current with the linear time course, $I(t) = a \cdot t$, and to obtain the integral

$$V(L, T) = C_0 \cdot a \int_0^T \frac{(T-t)}{\sqrt{t}} e^{(-L^2-4t^2)/4t}\, dt. \qquad (2)$$

The slope of the voltage change with respect to time is obtained by differentiating the above equation:

$$\frac{dV(L, T)}{dT} = C_0 \cdot a \int_0^T \frac{e^{(-L^2-4t^2)/4t}}{\sqrt{t}}\, dt. \qquad (3)$$

We are interested in the slope only after the voltage change has achieved linearity, at which time further increases in t will not alter the slope. For our purposes, then, we consider $T \to \infty$ and obtain

$$C_0 \int_0^\infty \frac{e^{(-(L^2+4t^2)/4t}}{\sqrt{t}}\, dt = \frac{Q_0}{2\lambda c_m} e^{-L}, \qquad (4)$$

where $Q_0/(2\lambda c_m)$ is constant (Jack et al., 1975, Eq. 3.52).

Under these conditions, we find that if a voltage generated at a certain point is changing linearly with respect to time with slope a_1, the voltage recorded at electrotonic distance L from this point will have slope a_2 equal to $a_1 e^{-L}$. Therefore, $L = -\ln(a_2/a_1)$.

References

Amitai Y, Friedman A, Connors BW, Gutnick MJ (1993) Regenerative electrical activity in apical dendrites of pyramidal cells in neocortex. Cereb Cortex 3:26–38.

Benardo LS, Masukawa LM, Prince DA (1982) Electrophysiology of isolated hippocampal pyramidal dendrites. J Neurosci 2:1614–1622.

Brown AM, Schwindt PC, Crill WE (1992) Kinetics and voltage dependence of the high threshold calcium current in rat neocortical neurons. Soc Neurosci Abstr 18:430.

Cauller LJ, Connors BW (1992) Functions of very distal dendrites: experimental and computational studies of layer 1 synapses on neocortical pyramidal cells. In: Single neuron computation (McKenna T, Davis J, Zornetzer SF, eds), pp 199–229. Boston: Academic.

Connor JA, Wadman WJ, Hockberger PE, Wong RK (1988) Sustained dendritic gradients of Ca^{2+} induced by excitatory amino acids in CA1 hippocampal neurons. Science 240:649–653.

Connors BW, Gutnick MJ, Prince DA (1982) Electrophysiological properties of neocortical neurons *in vitro*. J Neurophysiol 48:1302–1320.

Connors BW, Benardo LS, Prince DA (1984) Carbon dioxide sensitivity of dye coupling among glia and neurons of the neocortex. J Neurosci 4:1324–1330.

Dichter MA, Zona C (1989) Calcium currents in cultured rat cortical neurons. Exp Brain Res 492:219–229.

Dimitrova NA, Dimitrov GV (1991) Difference in excitability along geometrically inhomogeneous structures and occurrence of hot spots. Biol Cybern 66:185–189.

Fitzhugh R (1960) Thresholds and plateaus in Hodgkin-Huxley nerve equations. J Gen Physiol 43:867–896.

Franz P, Galvan M, Constanti A (1986) Calcium-dependent action potentials and associated inward currents in guinea-pig neocortical neurons *in-vitro*. Brain Res 366:262–271.

Friedman A, Gutnick MJ (1987) Low-threshold calcium electrogenesis in neocortical neurons. Neurosci Lett 81:117–122.

Friedman A, Gutnick MJ (1989) Intracellular calcium and control of burst generation in neurons of guinea-pig neocortex *in vitro*. Eur J Neurosci 1:374–381.

Friedman A, Arens J, Heinemann U, Gutnick MJ (1992) Slow depolarizing afterpotentials in neocortical neurons are sodium and calcium dependent. Neurosci Lett 135:13–17.

Gutnick MJ, Prince DA (1981) Dye coupling and possible electrical coupling in the guinea pig neocortical slice. Science 211:67–70.

Gutnick MJ, Lobel-Yaakov R, Rimon G (1985) Incidence of neuronal dye-coupling in neocortical slices depends on the plane of section. Neuroscience 15:659–666.

Gutnick MJ, Lux HD, Swandulla D, Zucker H (1989) Voltage-dependent and calcium-dependent inactivation of calcium current in identified snail neurones. J Physiol (Lond) 412:197–220.

Harris NC, Ramsay S, Kelion A, Greenfield SA (1989) Electrophysiological evidence for the dendritic localization of a calcium conductance in guinea-pig substantia nigra neurones *in vitro*. Exp Brain Res 74:411–416.

Hillman D, Chen S, Aung TT, Cherksey B, Sugimori M, Llinas RR (1991) Localization of P-type calcium channels in the central nervous system. Proc Natl Acad Sci USA 88:7076–7080.

Hines M (1989) A program for simulation of nerve equations with branching geometries. Int J Biomed Comput 24:55–68.

Hodgkin AL, Keynes R (1957) Movement of labelled calcium in squid giant axons. J Physiol (Lond) 138:253–281.

Hodgkin AL, Rushton WAH (1946) The electrical constants of a crustasean nerve fibre. Proc R Soc Lond [Biol] 133:444–479.

Huguenard JR, Prince DA (1992) A novel T-type current underlies prolonged Ca^{2+}-dependent burst firing in GABAergic neurons of rat thalamic reticular nucleus. J Neurosci 12:3804–3817.

Huguenard JR, Hamill OP, Prince DA (1989) Sodium channels in dendrites of rat cortical pyramidal neurons. Proc Natl Acad Sci USA 86:2473–2477.

Imredy JP, Yue DT (1992) Submicroscopic Ca^{2+} diffusion mediates inhibitory coupling between individual Ca^{2+} channels. Neuron 9:197–207.

Jack JJB, Redman SJ (1971) The propagation of transient potentials in some linear cable structures. J Physiol (Lond) 215:283–320.

Jack JJB, Noble D, Tsien RW (1975) Electric current flow in excitable cells. London: Oxford UP.

Jaffe DB, Johnston D, Lasser-Ross N, Lisman JE, Miyakawa H, Ross WN (1992) The spread of Na spikes determines the pattern of dendritic Ca entry into hippocampal neurons. Nature 357:244–246.

Jahnsen H, Llinas R (1984) Ionic basis for the electro-responsiveness and oscillatory properties of guinea-pig thalamic neurones *in vitro*. J Physiol (Lond) 349:227–247.

Jones OT, Kunze DL, Angelides KJ (1989) Localization and mobility of omega-conotoxin-sensitive Ca^{2+} channels in hippocampal CA1 neurons. Science 244:1189–1193.

Kay AR (1991) Inactivation kinetics of calcium current of acutely dissociated CA1 pyramidal cells of the mature guinea-pig hippocampus. J Physiol (Lond) 437:27–48.

Kay AR, Wong RK (1987) Calcium current activation kinetics in isolated pyramidal neurones of the CA1 region of the mature guinea-pig hippocampus. J Physiol (Lond) 392:603–616.

Kohr G, Mody I (1991) Endogenous intracellular calcium buffering and the activation/inactivation of HVA calcium currents in rat dentate gyrus granule cells. J Gen Physiol 98:941–967.

Krnjevic K, Pumain R, Renaud L (1971) Effects of Ba^{2+} and tetraethylammonium on cortical neurones. J Physiol (Lond) 215:223–245.

Larkman AU, Major G, Stratford KJ, Jack JJ (1992) Dendritic morphology of pyramidal neurones of the visual cortex of the rat. IV: Electrical geometry. J Comp Neurol 323:137–152.

Leonard JP, Wickelgren WO (1985) Calcium spike and calcium-dependent potassium conductance in mechanosensory neurons of the lamprey. J Neurophysiol 53:171–182.

Lev-Ram V, Miyakawa H, Lasser-Ross N, Ross WN (1992) Calcium transients in cerebellar Purkinje neurons evoked by intracellular stimulation. J Neurophysiol 68:1167–1177.

Llinas R, Nicholson C (1971) Electroresponsive properties of dendrites and somata in alligator Purkinje cells. J Neurophysiol 34:532–551.

Llinas R, Sugimori M (1980) Electrophysiological properties of *in vitro* Purkinje cell dendrites in mammalian cerebellar slices. J Physiol (Lond) 305:197–213.

Llinas R, Yarom Y (1981) Properties and distribution of ionic conductances generating electroresponsiveness of mammalian inferior olivary neurones *in vitro*. J Physiol (Lond) 315:569–584.

Llinas RR, Sugimori M, Cherksey B (1989) Voltage-dependant calcium conductances in mammalian neurons (the P channel). Ann NY Acad Sci 560:103–111.

Lorente de No R, Condouris G (1959) Decremental conduction in peripheral nerve. Integration of stimuli in the neuron. Proc Natl Acad Sci USA 45:592–617.

Masukawa LM, Prince DA (1984) Synaptic control of excitability in isolated dendrites in hippocampal neurons. J Neurosci 4:217–227.

McBurney RN, Neering IR (1987) Neuronal calcium homeostasis. Trends Neurosci 10:164–169.

Noble D, Tsien RW (1969) Reconstruction of the repolarization process in cardiac Purkinje fibres based on voltage clamp measurements of membrane current. J Physiol (Lond) 200:233–254.

Pennefather P, Sala F, Hernandez-Cruz A (1990) Computer simulation of I_{AHP} kinetics. Soc Neurosci Abstr 16:187.

Rall W (1977) Core conductance theory and cable properties of neurons. In: Handbook of physiology, Sec 1, The nervous system, Vol 1 (Kandel ER, ed), pp 39–38. Bethesda, MD: American Physiological Society.

Reuveni I, Friedman A, Gutnick MJ (1992) Non-homogenous distribution of calcium electrogenesis along the dendrites of neocortical pyramidal neurons. Soc Neurosci Abstr 18:848.

Ross WN, Werman R (1987) Mapping calcium transients in the dendrites of Purkinje cells from the guinea-pig cerebellum *in vitro*. J Physiol (Lond) 389:319–336.

Ross WN, Lasser-Ross N, Werman R (1990) Spatial and temporal analysis of calcium-dependent electrical activity in guinea pig Purkinje cell dendrites. Proc R Soc Lond [Biol] 240:173–185.

Sayer RJ, Schwindt PC, Crill WE (1990) High-threshold and low-threshold calcium currents in neurons acutely isolated from rat sensorimotor cortex. Neurosci Lett 120:175–178.

Schwindt PC, Spain W, Foehring RC, Stafstrom CE, Chubb MC, Crill WE (1988a) Multiple potassium conductances and their functions in neurons from cat sensorimotor cortex *in vitro*. J Neurophysiol 59: 424–449.

Schwindt PC, Spain W, Foehring RC, Stafstrom CE, Chubb MC, Crill WE (1988b) Slow conductances in neurons from cat sensorimotor cortex *in vitro* and their role in slow excitability changes. J Neurophysiol 59:450–467.

Segev I, Fleshman JW, Burke RE (1989) Compartmental models of complex neurons. In: Methods in neuronal modelling (Koch C, Segev I, eds), pp 171–194. Cambridge, MA: MIT Press.

Stafstrom CE, Schwindt PC, Crill WE (1984) Properties of subthreshold response and action potential recorded in layer 5 neurons from cat sensorimotor cortex *in vitro*. J Neurophysiol 52:244–263.

Stafstrom CE, Schwindt PC, Chubb MC, Crill WE (1985) Properties of persistent sodium conductance and calcium conductance of layer V neurons from cat sensorimotor cortex *in vitro*. J Neurophysiol 53: 153–170.

Stratford K, Mason A, Larkman A, Major G, Jack JJB (1989) The modeling of pyramidal neurones in the visual cortex. In: The computing neuron (Durbin R, Mial C, Mitchison G, eds), pp 296–321. Menlo Park, CA: Addison-Wesley.

Sugimori M, Llinas RR (1990) Real-time imaging of calcium influx in mammalian cerebellar Purkinje cells *in vitro*. Proc Natl Acad Sci USA 87:5084–5088.

Sutor B, Zieglgansberger W (1987) A low-voltage activated, fully inactivated, transient calcium current is responsible for the time-dependent depolarizing inward rectification of rat neocortical neurons *in-vitro*. Pfluegers Arch 410:102–111.

Swanson G, ed (1989) Special issue: calcium-effector mechanisms. Trends Neurosci 12:417–478.

Tank DW, Sugimori M, Connor JA, Llinas RR (1988) Spatially resolved calcium dynamics of mammalian Purkinje cells in cerebellar slice. Science 242:773–777.

Tsien RW, Lipscombe D, Madison DV, Bley KR, Fox AP (1988) Multiple types of neuronal calcium channels and their selective modulation. Trends Neurosci 11:431–438.

Tsien RW, Ellinor PT, Horne HA (1991) Molecular diversity of voltage dependent Ca^{2+} channels. Trends Pharmacol 12:349–354.

Westenbroek RE, Ahlijanian MK, Catterall WA (1990) Clustering of L-type Ca^{2+} channels at the base of major dendrites in hippocampal pyramidal neurons. Nature 347:281–284.

Westenbroek RE, Hell JW, Concepcion W, Dubel SJ, Snutch TP, Catterall WA (1992) Biochemical properties and subcellular distribution of an N-type calcium channel $\alpha 1$ subunit. Neuron 9:1099–1115.

Wilson DL, Morimoto K, Tsuda Y, Brown AM (1983) A quantitative analysis of surface charge effects on gating permeation of the calcium channel. J Membr Biol 72:117–130.

Wong RKS, Prince DA, Basbaum AI (1978) Intradendritic recordings from hippocampal neurons. Proc Natl Acad Sci USA 76:986–990.